J Mater Sci (2009) 44:4728–4733
DOI 10.1007/s10853-009-3731-1

Microtensile tests of mechanical properties of nanoporous Au thin films

Re Xia · Caixia Xu · Wenwang Wu · Xide Li · Xi-Qiao Feng · Yi Ding

Received: 28 February 2009 / Accepted: 4 July 2009 / Published online: 22 July 2009

Abstract The mechanical properties of nanoporous Au (NPG) thin films were investigated by uniaxial microtensile tests. Such mechanical parameters as Young's modulus, tensile strength, and breaking strain were obtained from the recorded force–displacement curves. Through observations on the microstructure and fracture surface morphology of the samples after the tension tests by a scanning electronic microscope (SEM) and an optical microscope, we analyzed the physical mechanisms underlying the mechanical behavior of NPG thin films. It was found that the NPG films exhibit mechanical properties distinctly different from its bulk counterpart.

Introduction

Nanoporous materials have gained considerable attention because of their potential applications in actuation, catalysis, sensing, filtration, and tissue engineering [1–4]. Nanoporous Au (NPG), as a well-known material in this category, is a particular candidate for studying the mechanical behavior of nanoporous metals due to its easy fabrication and remarkable stability against corrosion and oxidation [5–7]. Li and Sieradzki [8] investigated the ductile-brittle transition of random porous Au by observing its deformation and fracture behavior under different sample sizes and ligament length scales. Such mechanical parameters as the yield strength and elastic modulus of NPG have also been measured by compression or bending tests [9–12]. Recently, the influence of annealing temperature on the microstructure and mechanical behavior of NPG films was also studied [13–15]. The measured yield strength and elastic modulus show a distinct dependence on the characteristic sizes of microstructure and are larger than those theoretically predicted by the scaling equations developed for macroscopic open-cell and closed-cell foams [7, 16]. The ligament size dependence of elastic properties of NPG can be attributed to the surface effects [17]. However, there is still a lack of direct mechanical measurement by using uniaxial tension tests for NPG films with a thickness of several or tens micrometers.

As is well-known, uniaxial tension test has some prominent advantages in characterization of the mechanical properties of thin film materials. It provides readily interpretable data and uniaxial stress–strain curves and allows direct extraction of such mechanical parameters as elastic modulus, tensile strength, and yield stress [18, 19] under different loading environments [20]. Although macroscopic tensile and compressive tests are conventional to measure the mechanical properties of metallic foams [21, 22], the direct tensile test of NPG films is still difficult due to their fragile feature. In the present article, we report a novel microtensile system to measure the mechanical properties of NPG films. The microscopic mechanisms underlying the deformation and failure behaviors of NPG films are also analyzed.

R. Xia · W. Wu · X. Li (✉) · X.-Q. Feng (✉)
Department of Engineering Mechanics, AML,
Tsinghua University, Beijing 100084, China
e-mail: lixide@tsinghua.edu.cn

X.-Q. Feng
e-mail: fengxq@tsinghua.edu.cn

C. Xu · Y. Ding
School of Chemistry and Chemical Engineering,
Shandong University, Jinan 250100, China

Materials and experimental procedure

An NPG sample can be fabricated by chemical or electrochemical dissolution of Ag atoms from a miscible Au–Ag alloy, and it typically has an open-cell and fully interconnected network structure consisting of Au ligaments and nanosized pores [23]. In this study, the material for preparing NPG samples was a homogenized $Au_{28}Ag_{72}$ (at.%) alloy ingot, which was first rolled to a film and then annealed in air at 850 °C for 3 h. In comparison with the effect of post-dealloying annealing, the influence of pre-annealing on the elastic properties of the NPG can be ignored [14, 15]. The films (or foils) were dealloyed by free corrosion using concentrated HNO_3 ($\sim$67%) for 30 min at room temperature, and then washed with de-ionized water, and finally dried in the air. Compositional analysis using energy dispersive X-ray spectroscopy (EDS) confirmed that the residual silver concentration was less than 8%. The dealloyed structure is shown in Fig. 1. The grain structure has an average grain size of 10 μm and each grain contains dozens of sub-grains whose size ranges from 120 nm to 1 μm. The foam has a typical ligament diameter about $t = 10$–11 nm and cell size about $l = 20$ nm. An approximate value of the relative density of an open-cell foam material can be calculated by $\rho/\rho_s = (t/l)^2 = 30\%$, where ρ and ρ_s are the mass density of foam and the nonporous solid framework, respectively [16]. There are about 130 nanovoids in the view range of 250 × 250 nm^2. This yields the side length to be 21.9, 16.7, or 13.6 nm if the planar geometric configuration of the cell is assumed to have the equilateral quadrangle, pentagon, or hexagon, respectively. It is seen that the equilateral quadrangle's value is in good consistence with the cell sizes estimated from SEM images. In our tension tests, the NPG film of 20 ± 2 μm in thickness was cut as rectangular samples with the average dimensions of 1 ± 0.1 mm (length) and 0.2 ± 0.04 mm (width).

We developed a uniaxial microtensile system for measuring the properties of NPG films. Figure 2a shows its photograph under an optical microscope during the test. The tensile system consists of four main parts, namely, the mechanical frame, the PZT ceramic actuating unit, the force sensing unit, and the sample stage. The mechanical frame, as the support of the system, is a U-type structure made of aluminum alloy. The PZT actuating unit consists of four cylinder translation bars, two sliding blocks and two PZT actuators. The two slides, with one end connected to the PZT actuator and the other to the supporting spring, are driven by the PZT actuators and can glide symmetrically in the two opposite directions along the cylinder translation bars. The force sensing unit consists of two force sensors in a type of double-cantilever beams, which are connected to the slides with their fixed ends and to the sample stages with their free ends. A programmable control unit was utilized to drive the actuators continually or step by step with DC voltage varying from 0 to 200 V with a resolution of 0.05 V. The actuators can produce the maximum displacement of about 100 μm (or the maximum force of

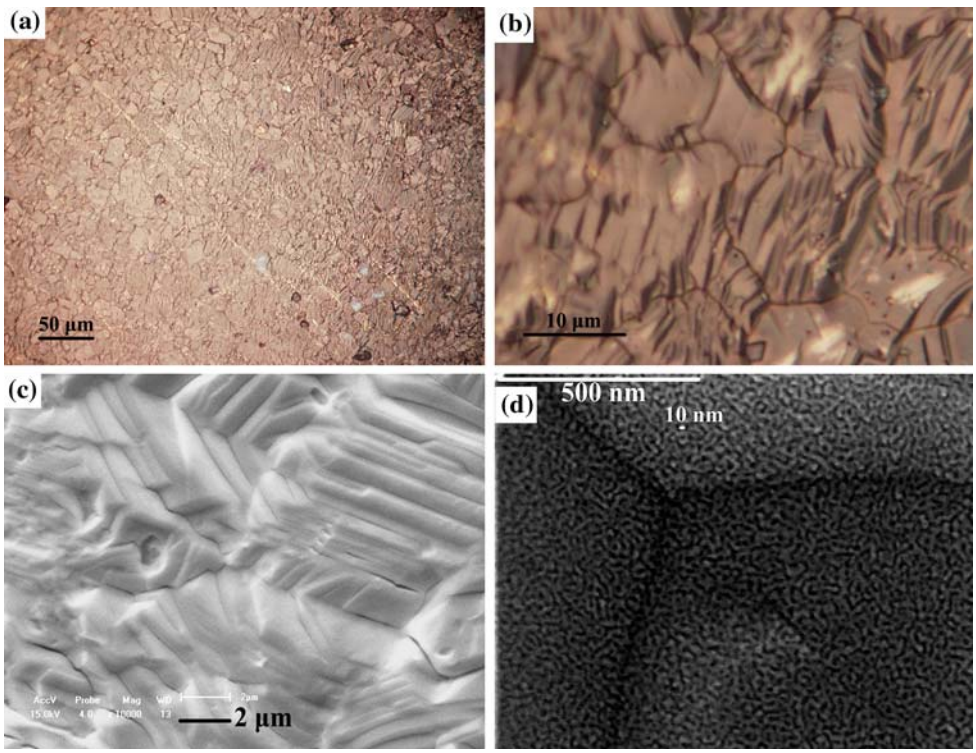

Fig. 1 Surface morphology of NPG under different magnifications: **a** and **b** optical images, **c** and **d** SEM images

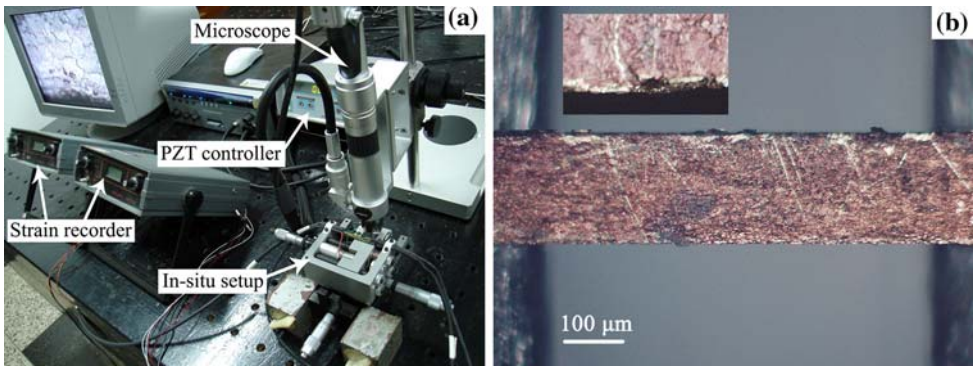

Fig. 2 **a** Photograph of in situ uniaxial tension system. **b** Image of a sample mounted on the sample stages of the uniaxial tension system

about 625 N), with a displacement resolution of several nanometers. The capacity of the used force sensor is 15 N with the resolution of 0.3 mN.

Fixation and alignment of the sample in the testing machine is a key step before the experiment. An NPG sample was glued to the clamp ends of the sample stages which are connected to the double-cantilever force sensors. The alignment of the sample and the grips was conducted under an optical microscope (model KH-3000, HiRox, Japan), ensuring the axes of the film and the grips to be identical (see Fig. 2b). During the experiment, the tensile load was gradually applied to the sample under the condition of displacement control mode at room temperature. Sequential images of the sample surface were captured during the tensile process in order to investigate the deformation and failure mechanisms. Since the small clearance and misalignment between the sample and grips may cause some errors in the results, we do not calculate the sample deformation from the displacements of sample stages. Instead, the relative displacement of two marker points with special characteristics and at the same horizontal line (along the tensile direction) on the sample surface is used to measure the sample displacements during loading. The displacement or elongation rate of the film along the tensile direction is determined with one pixel accuracy from the changes in the span length defined by the selected two marker points. This method allows us to exactly determine the tensile displacements. In addition, a series of voltages driving the actuators were simultaneously recorded to determine the forces applied to the sample.

Results and discussions

The experimental results of our tests are summarized in Table 1, and four typical load–displacement and engineering stress–strain curves are given in Fig. 3. The

Table 1 Summary of the measured properties of NPG thin films

Samples	Young's modulus (GPa)	Yield strength (MPa)	Ultimate tensile strength (MPa)	Breaking strain (%)
Sample 1	12.5	62.1	90.2	7.3
Sample 2	12.6	56.7	87.6	6.8
Sample 3	12.4	62.3	97.9	6.2
Sample 4	12.6	57.7	67.4	2.4

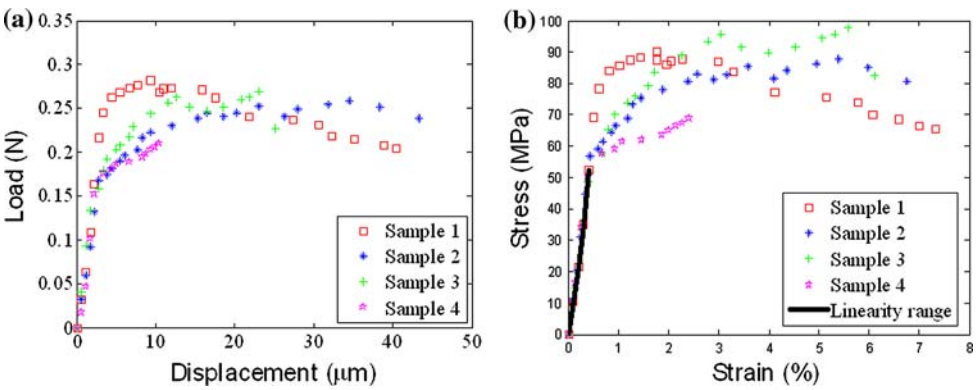

Fig. 3 Experimental results: **a** load–displacement curves, **b** engineering stress–strain curves

deformations of the tested NPG films are approximately linear with the increasing load at the initial stage, and the linear elastic stages of different samples are in a good consistency. Taken from the first loading portion of the curves, the Young's modulus, E, of the material is determined as 12.5 ± 0.1 GPa, close to 11.1 ± 0.9 GPa measured by nanoindentation tests [9] and in the range of 10.1–15.0 GPa calculated by Gibson–Ashby's scaling laws developed for open-cell foams $E = E_S(\rho/\rho_S)^2$, where E_S is the Young's modulus of solid Au and in the range from 57 to 85 GPa [9]. The small dispersion of Young's modulus obtained from our tests is attributed to the relatively uniform nanoporous structure of the material and the relatively large size of the adopted samples. The effective Young's modulus, E, of a tensile sample basically depends upon the statistical distribution of microstructure parameters (e.g., pore and ligament size) but is insensitive to the concrete sizes and locations of individual nanovoids. Therefore, E shows a weak size effect and small scatter provided that the samples are sufficiently large in comparison with the characteristic dimensions of material microstructures.

The plastic yielding of the material happens at the strain of about 0.4 ± 0.1%, followed by a strain-hardening stage and a softening stage. The measured yield stresses, σ_S, are in the range of 59.7 ± 3.0 MPa. Using the nanoindentation method, Biener et al. [7, 9] measured the hardness values of micrometer-sized NPG columns, e.g., 171 ± 35 GPa for 30% NPG with 10 nm ligaments. Our results fit well with those of Biener et al. [7], if we adopt the recently elaborated relation between hardness and yield strength [24], $H = 3\sigma_s$.

Also from the uniaxial tensile curves of the samples 1–3, we obtained the ultimate tensile strength, defined as the maximum stress the material can bear, in the range from 87.6 to 97.9 MPa and the elongation rate in the range from 6.2 to 7.3%. However, it is noteworthy that the tensile strength and elongation of the sample 4 are pronouncedly lower than those of the other samples. To interpret this derivation, we carefully observed and compared the images of the sample surfaces before test. We found that there was a small notch on one side of the sample 4 (see the inset of Fig. 2b). Because of the brittle property of the NPG material, the tensile strength and elongation rate are sensitive to the presence of surface defects, which may be introduced during the process of dealloying and sample preparing. Therefore, the measured ultimate tensile strength and elongation rate may be pronouncedly lowered by surface defects. The stress concentration near a defect may induce the nucleation of a crack and the final breakage of the sample at a relatively low stress level.

In our uniaxial microtensile tests, the size of the samples is much larger than the characteristic sizes of pores, ligaments, and grains, thus obtaining relatively uniform stress distribution and small dispersion of the measured effective or averaged properties of porous materials. However, the ultimate strength and the elongation rate of one sample show a relatively larger dispersion. These failure-related properties are sensitive to the sizes, locations, and orientations of individual microcracks, namely, the extreme values of defect distributions rather than the statistically averaged parameters. The fracture behavior of the NPG samples can be explained by the weakest link theory [25]. Although the average size of nanovoids and other defects are in good consistency for different samples, the extreme defect parameters (e.g., the maximum size of defects) or the weakest links in them may have a distinct difference from the stochastic viewpoint [26]. The acid treatment and sample preparing of NPG samples may induce microcracking, which, in turn, results in a decrease in the measured tensile strength. The volume shrinkage following dealloying may also cause residual stress at the microstructural level and accelerate the nucleation of microcracks. For these reasons, both increasing the Au content in the Au–Ag alloy and the multi-step dealloying treatment process influence the plastic yield and failure behavior of the material [27, 28].

To further explore the fracture mechanisms of NPG films, the global fracture process of NPG films was also carefully observed during microtensile tests. Figure 4 gives a typical fracture pattern near the midpoint of the samples. A crack initiated from one edge of the sample and then propagated along grain boundaries or through the grains themselves, exhibiting a mixed intergranular and transgranular failure mode. The intergranular rupture mechanism was dominant during the rupture process, and the transgranular fracture was observed only in small regions including a few grains, as is similar to the failure mode observed in microporous materials [29]. The rupture mechanisms are understandable by considering the local deformations around a microcrack located between two neighboring grains, and the microcrack is apt to advance along the relatively weaker interfaces [30]. For nanoporous materials, intergranular cracking is relatively easier than transgranular failure because of the weak constraint effect of grains. With the increase in the applied force, some deformation and damage phenomena (e.g., grain boundary widening, microcrack propagating and linking, and subdivision of grains) were observed in a small region around the crack tip. Large-scale sliding process associated with plastic deformation was not found in the experiments. The stress concentration near the crack tip induces the formation of some new interface microcracks around and nearby the grains. The microcracks grew and propagated gradually, yielding a network of microcracks. Finally, a main crack is formed as a consequence of microcrack coalescence. Its unstable propagation led to the final rupture of

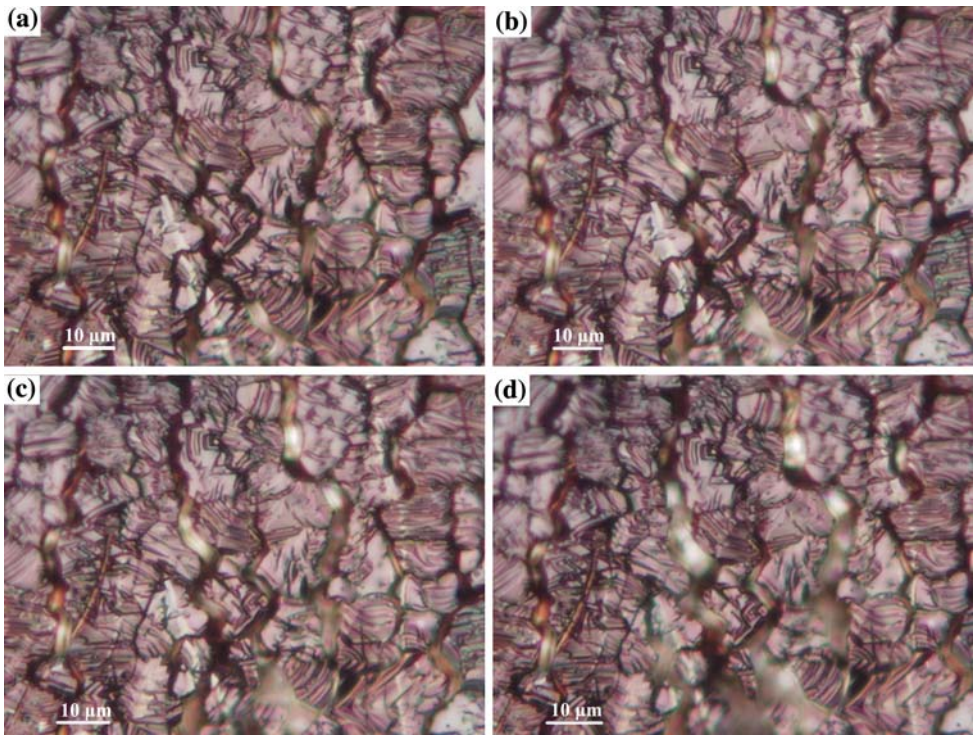

Fig. 4 Optical images of crack growth and grain deformation

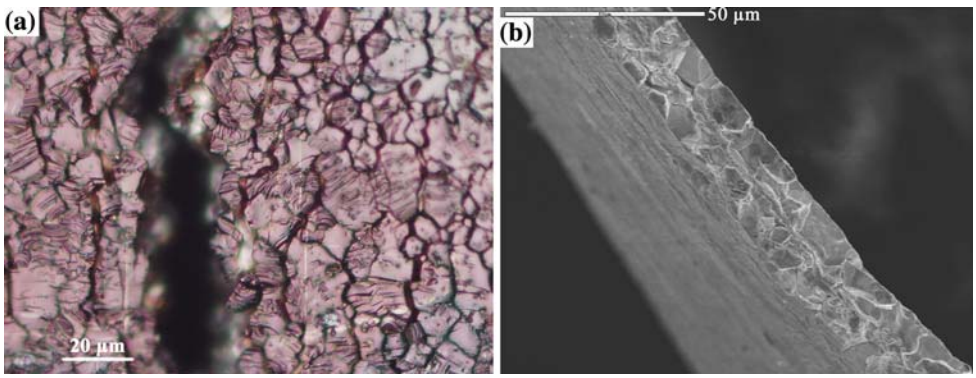

Fig. 5 Fracture surface of a sample after the tension test: **a** optical image, **b** SEM image

the sample. Figure 5 gives the fracture surface of a sample, which is flat and shiny, indicating an intergranular fracture.

Summary

In summary, quasi-static uniaxial tension tests of nanoporous Au thin films have been carried out by using a home-made micro-tension setup under an optical microscope. The average tensile modulus and yield stress of the NPG material are 12.5 GPa and 59.7 MPa, respectively. The global fracture process was recorded in real-time in order to analyze and interpret the fracture features of NPG material. Further theoretical modeling on the mechanical behavior and physical mechanisms is of great interest and will be conducted in the next step.

Acknowledgements This study is supported by the NSFC (grants No. 10572071, 10732080, and 10525210), the National Basic Research Program of China (grant No. 2007CB936803 and 2004CB619304), the Ministry of Education (grant No. 20070003053), and the Central Laboratory of Strength and Vibration of Tsinghua University. YD is a Tai-Shan Scholar supported by the SEM-NCET and SRF-ROCS Programs.

References

1. Weissmüeller J, Viswanath RN, Kramer D, Zimmer P, Wuerschum R, Gleiter H (2004) Science 300:312
2. Erlebacher J, Aziz MJ, Karma A, Dimitrov N, Sieradzki K (2001) Nature (Lond) 410:450
3. Kramer D, Viswanath RN, Weissmueller J (2004) Nano Lett 4:793
4. Ganguly P, Ulm F-J (2007) J Mater Res 42:8873
5. Ding Y, Chen M, Erlebacher J (2004) J Am Chem Soc 126:6876

6. Xu CX, Su JX, Xu XH, Liu PP, Zhao HJ, Tian F, Ding Y (2007) J Am Chem Soc 129:42
7. Biener J, Hodge AM, Hayes JR, Volkert CA, Zepeda-Ruiz LA, Hamza AV, Abraham FF (2006) Nano Lett 6:2379
8. Li R, Sieradzki K (1992) Phys Rev Lett 68:1168
9. Biener J, Hodge AM, Hamza AV, Hsiung LM, Satcher JH (2005) J Appl Phys 97:024301
10. Volkert CA, Lilleodden ET, Kramer D, Weissmüller J (2006) Appl Phys Lett 89:061920
11. Hakamada M, Mabuchi M (2007) Scr Mater 56:1003
12. Lee D, Wei X, Chen X, Zhao M, Jun SC, Hone J, Herbert EG, Oliver WC, Kysar JW (2007) Scr Mater 56:437
13. Sun Y, Kucera KP, Burger SA, Balk TJ (2008) Scr Mater 58:1018
14. Seker E, Gaskins JT, Smith HB, Zhu J, Reed ML, Zangari G, Kelly R, Begley MR (2007) Acta Mater 55:4593
15. Seker E, Gaskins JT, Smith HB, Zhu J, Reed ML, Zangari G, Kelly R, Begley MR (2008) Acta Mater 56:324
16. Gibson LJ, Ashby MF (1997) Cellular solids: structures and properties, 2nd edn. Cambridge University Press, Cambridge
17. Feng XQ, Xia R, Li XD, Li B (2009) Appl Phys Lett 94:011916
18. Avilés F, Llanes L, Oliva AI (2009) J Mater Sci 44:2590. doi: 10.1007/s10853-009-3339-5
19. Ahn B, Lavernia EJ, Nutt SR (2008) J Mater Sci 43:7403. doi: 10.1007/s10853-008-2950-1
20. Ruggles-Wrenn MB, Koutsoukos P, Baek SS (2008) J Mater Sci 43:6734. doi:10.1007/s10853-008-2784-x
21. Marchi CS, Despois JF, Mortensen A (2004) Acta Mater 52:2895
22. Amsterdam E, de Vries JHB, De Hosson JTM, Onck PR (2008) Acta Mater 56:609
23. Ding Y, Kim YJ, Erlebacher J (2004) Adv Mater 16:1897
24. Jin HJ, Kurmanaeva L, Schmauch J, Rösner H, Ivanisenko Y, Weissmüller J (2009) Acta Mater 57:2665
25. McCullough KYG, Fleck NA, Ashby MF (1999) Acta Mater 47:2323
26. Feng XQ, Li JY, Yu SW (2003) Int J Solids Struct 40:447
27. Lu X, Balk TJ, Spolenak R, Arzt E (2007) Thin Solid Films 515:7122
28. Sun Y, Balk TJ (2008) Scr Mater 58:727
29. Amsterdam E, Onck PR, De Hosson JTM (2005) J Mater Sci 40:5813. doi:10.1007/s10853-005-4995-8
30. Haque MA, Saif MTA (2004) PNAS 101:6335